Contour-Based Personalisation of Human Body Models

Aditya Chhabra, Anoop Chawla, Sudipto Mukherjee, Akhilesh Choudhary

Abstract Finite Element Human Body models have emerged as a cost-effective alternative to Anthropometric Test Devices (ATDs) [1] for crash testing and play a pivotal role in design for crash safety, by providing accurate predictions of human response to impacts. The ability to generate HBMs of varying anthropometry from an existing HBM shall enable vehicle safety studies for a wider range of body types.. This paper presents an approach for personalisation of Human Body Models (HBMs) using contours, a technique that was previously used to create Posture-Specific Human Body models in Chhabra *et al.* [39]. The mesh creation is verified by comparing the elemental Jacobian ratio, aspect ratio, and the interior angles of the generated model with that of the nominal HBM to establish confidence in use of the model when running explicit FE simulations.

Keywords Human Body Models, HBM Personalisation, Contour Generation, Delaunay Tetrahedralisation, Anthropometric Parameter Estimation.

I. INTRODUCTION

Crash testing has played a crucial part in ensuring crash safety over the last five decades, but it remains an expensive process. A significant cost factor in crash testing is the use of crash test dummies or full-scale ATDs [1]. These ATDs are metal-and-polymer constructs that are expensive to manufacture and calibrate, which is why they are available only in a limited number of shapes and sizes. To represent the diversity in the population and to minimise the cost associated with crash testing, crash simulation using models of the human and the vehicle [2] has emerged as a viable alternative. These simulations reproduce real-world injury patterns and finer resolution of the crash consequences than tests using ATDs. Recently, the gold standard for crash simulators [3-5] includes the use of Finite Element Human Body Models (FE-HBMs), which can represent subjects of differing body dimensions, weights, etc. The creation of these FE-HBMs for varying Anthropometric Parameters [6] (AP) has been time-consuming and required significant human intervention. Therefore, there is a need to modify nominal FE-HBMs to generate an FE-HBM of specified anthropometry. Though anthropometry are surface measurements, the modification targeted towards them needs to percolate down to the organ level while maintaining numerical stability when running explicit FE analysis.

Currently, the HBMs with limited anthropometric combinations (e.g. 5^{th} percentile female, 50^{th} and 95^{th} percentile male of the global population) are available for crash simulations. These HBMs do not span the anthropometric variety of the vehicle users or pedestrian populations. Given that the efficacy of the safety measures, changes with anthropometry, availability of HBMs of different anthropometries is important in vehicle safety studies [7-9] using crash simulations [10-11]. Some of the FE HBMs that are commercially available include the THUMS model [12-15], the GHBMC model [16], the HUMOS model [17], the SAFER-HBM [18-19] and the PIPER child model [20-22] to name a few. These models capture the geometries of structurally complex human body parts, including the head, torso, joints and organs, by millions of finite elements [23]. This is a time-consuming task, and it is not feasible to repeat the task for every desired anthropometry. Therefore, personalisation processes have been developed to modify a reference HBM and obtain a model representing a person with specified anthropometry. The human body is a continuous structure, however, it is not intrinsically segmented into parts, as in ATDs. This increases the complexity of the personalisation process, as there is a need to ensure compatibility in the mesh between adjacent body regions. In addition, the reference often needs to be repositioned to represent the posture of the target person, as the reference HBM is typically available limited postures. In this process of model modification, it is also important to ensure that the personalised model is computationally stable, which requires minimising mesh distortions, or formation of poor-quality elements.

A. Chhabra (e-mail: adityachhabra.oct@gmail.com; tel: +91-9205327797) is a phD student in School of IT at Indian Institute of Technology (IIT) Delhi and S. Mukherjee and A. Chawla are Professors in the Department of Mechanical Engineering at Indian Institute of Technology (IIT) Delhi, India.

This personalisation process has been attempted using the Kriging technique [24], with radial basis function (RBF) as an interpolating function to enforce compatibility between the body parts during personalisation. In this approach, landmarks (control points or CPs) on the skin and skeleton/joints are identified on the baseline HBM (as the source) and their locations on target HBM are specified. The source and target landmarks should have a one-to-one correspondence between them. A 3-D displacement field throughout the entire space of human geometry is built. This displacement field is then applied to the baseline HBM to transform the source nodes to generate the target HBM. Appreciating the advantages and identifying the challenges related to this approach has been the first step for the development of new techniques for the personalisation of the HBMs.

Jolivet *et al.* [24] compared the performance of kriging and moving least square (MLS) [25] methods for the personalisation of HBMs. The authors observed that Kriging can be computationally expensive when many control points are used, especially for the detailed target geometry that is needed when the shape of bones and skin are to be captured, as is the case in HBMs. It can also lead to element quality issues (including inverted elements), preventing the use of these models for FE simulation. The best results (with similar distances to the target, i.e. less than 1.5 mm on average) were obtained for the MLS using a control spline formed by the control points and the kriging method using some relaxation in the target definition (nugget effect). However, the two approaches had very different computational costs: in some cases, the MLS was so computationally expensive that it would make its interactive use impracticable; by contrast, Kriging-based transformations were relatively inexpensive.

Janak *et al.* [26] use a strategy combining spatial subdivision and iterative subsampling that lowers computational costs and enables the creation of usable models. A set of control points (CPs), which consist of a mix of global (external geometry) and local (internal geometry), is used. They do not use CPs to modify the mesh internal to the organs, which are subsequently modified based on the resultant effects of exterior mesh deformations. Smoothing techniques are used to reduce the distortion of elements at the boundary. Subsampling and subdivision parameters, such as number of subdivisions, number of nodes per subdivision, and parameters to control mesh distortion at the boundaries of subdivisions, are tuned to ensure a good quality mesh in the final model. The paper suggested that the criteria that could help to select control points should be evolved. They discussed the interrelationship between the spatial distribution of control points, smoothness of the transformation, effects on the HBM element quality, need for relaxation in target definition, computational cost, and biomechanical response, all of which needed to be studied to help make optimal choices.

Hwang *et al.* [27] describe a mesh morphing method for the rapid generation of parametric HBMs based on external body surface geometry. Landmark-based RBF interpolation functions were used to convert the base HBM to other geometries. However, the algorithm takes two hours to generate the results. It also has a template-based HBM constraint that works only with the THUMS v 4.01 version. In a subsequent paper, Hwang *et al.* [28] employed a mesh morphing method to rapidly develop parametric HBMs that can represent a wide range of anthropometry. They developed Parametric THUMS (P-THUMS), which took age, sex, stature and BMI as input, and also generated Subject-specific THUMS (S-THUMS). They then compared the simulated results with post-mortem human subjects (PMHS) test data for four side-impact tests with two male PMHS of different body sizes. They showed that the P-THUMS exhibited a better correlation. The method took about 1.5 hours on a 64-bit Intel® Xeon® CPU with 16 GB of RAM to generate each target HBM. Overall, 2% elements fell below the Jacobian value of 0.7. The morphing process is computationally less expensive than other RBF-based techniques but still takes time in the order of hours as it was employed individually on ten body regions, each containing up to 10,000 landmarks.

Zhang *et al.* [29] improved the mesh morphing method presented by [28] using an RBF based on Thin Plate Spline function (RBF-TPS). The body was divided into five regions and morphed separately, then integrated to generate the final human model. This improved the time complexity of the mesh morphing technique. For the morphed models, less than 3% shell elements had Jacobian values less than 0.7. It took about 10 minutes for generating a morphed model from the baseline using a contemporary 8-core PC.

Larsson *et al.* [30] personalised the SAFER v9 HBM [20-21], representing a 50th percentile male, into two elderly females based on age, sex, stature and BMI parameters using the RBF method proposed by [29] to enhance individual kinematics prediction in a side impact. The results revealed that the morphed models showed better correlation with human body kinematics than the baseline HBM. Larsson *et al.* [31] morphed the same baseline HBM (SAFER v9 HBM) into 27 females and 27 males of different anthropometries. PIPER and UMTRI Parametric HBM64 were the two key HBM morphing tools used. While both methods modify the shape of a HBM using target

anthropometric parameters as input, they differ in how they personalise the HBM. The PIPER interface allows more details and a more convenient interface to specify target anthropometric parameters at the time of morphing, but it does not morph the internal body parts like, say, the rib cage consistent with age, sex or BMI parameters. The UMTRI HBM morphing takes age, sex, BMI and stature as input parameters and uses that to directly personalise the human body.

Liu *et al.* [32] presented a methodology to derive an adult male HBM, with the aim of studying seating discomfort, starting from the PIPER Child model, with the skin surface, spine and pelvis as targets. The geometry of the skeleton and skin of the derived model are quite close to the source data, with a distance error of less than 2.3 mm on the skeleton and an error of 7.6 mm on the skin, on average. No negative volume elements were detected in the morphed model. However, the Jacobian mesh quality of the generated model was found to be deteriorated compared to the original Child model.

John *et al.* [33] developed a new set of FE-HBMs (from average female 50F) for the analysis of sex-specific differences in injuries and to achieve a balance between computational overhead and the finer details in the model using mesh morphing. The body mesh was segmented and morphing was performed sequentially for efficient processing.

Li *et al.* [34] introduced a novel and efficient landmark-free method for personalising HBMs using image registration. This automated approach allows for rapid personalisation of HBMs to new subjects, incorporating the morphing of both the external body shape and skeletons to target body shapes of skin and skeleton generated using SMPL [35] and OSSO [36]. The resulting personalised HBMs have element quality comparable to the baseline. The image registration-based morphing method consists of three modules: (i) pre-processing; (ii) image registration pipeline; and (iii) post-processing. Pre-processing involves converting the skin and skeleton of the human body into binary images through voxelisation. The pipeline uses Demons registration to obtain a displacement field that represents the anatomical differences between the baseline HBM and target subject, which is then used to morph the baseline into a personalised HBM. Post-processing assesses the accuracy of the personalisation.

Personalising HBMs will encounter computational challenges, especially when using techniques like Kriging, RBF and moving least squares. Achieving a balance between computational complexity and efficiency remains a central challenge for accurate and swift HBM personalisation. Also, the requirement of specific baseline models for personalisation can impose constraints on the flexibility and generalisation of the personalisation process. Moreover, relying on particular HBM templates limits applicability, emphasising the challenge of accommodating diverse anthropometric characteristics. A computationally efficient, near real-time method is presented here by implementing a graph encoding that drives the sequence of operation. The use of stick-diagram type contour control lines, sectioning planes which are locally perpendicular to these lines, and Delauney Tetrahedralisation leads to an efficient encoding of the process of personalisation. The end process has minimal mesh quality degradation and runs in under 60 s on a standard workstation when evaluated with nine test cases.

II. METHODS

In a bid to address the limitations of previous approaches, a contour-based approach for the personalisation of HBMs was used. This method was introduced by Jani *et al.* [37-38] and later by Chhabra *et al.* [39] to reposition HBMs and create Posture-Specific HBMs. One of the key advantages of this methodology is its ability to personalise using independent scale factors for different body segments as well as from specified anthropometric parameters. Global geometric transformations are skirted in this approach and transformations are applied on a subset of contour points, and the HBM mesh is repositioned as a consequence of movement of contour points. The algorithm aims to keep the number of elements failing the mesh quality criteria kept close to that of the baseline HBM and tends to maintain the Shell Jacobian ratio [40-42] greater than 0.7, aspect ratio less than 3, interior angles within 20-160 degrees for hexahedral elements and between 15-150 degrees tetrahedral elements, for at least 95% of the elements [63-65]. The number of elements failing the criteria remains close to that in the baseline HBM. This approach has been implemented in the PIPER toolkit under the Contour Personalisation module. The proposed methodology comprises five steps, as shown in Fig. 1.

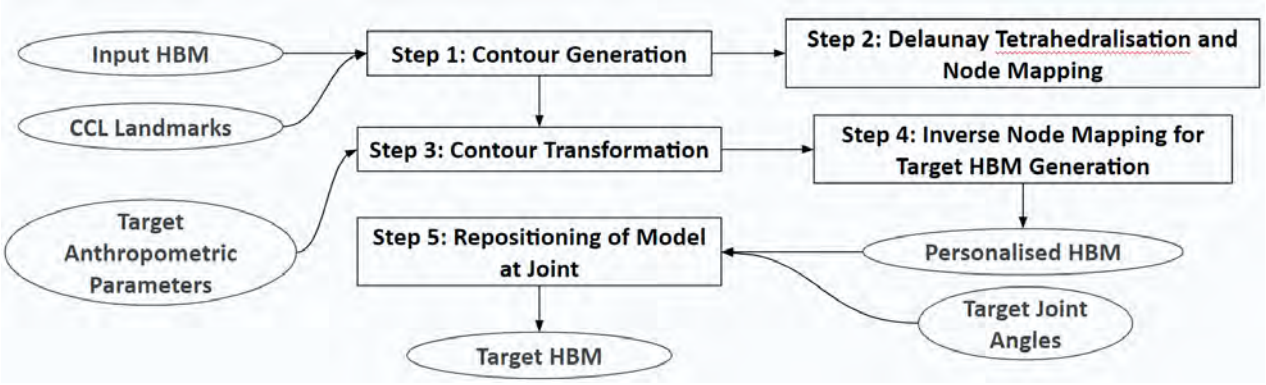

Fig. 1. Complete Pipeline of the HBM Modification methodology, Personalisation (Steps 1 to 4) followed by Repositioning (Step 5).

Step 1: Contour Generation

The first step involves generating a curve, called the contour control line (CCL or ContourCL shown by a white line in Fig. 2(b)), by joining a set of specially chosen anatomical landmarks, as detailed in [39]. These landmarks are manually selected from the set of bone nodes using the landmark picking tool available in the PIPER software framework [58-59]. The ContourCL is made of either linear segments or cubic splines for each body region (Fig. 2(b)). Body regions with long bones such as upper arms, forearms, thighs and calves have a linear ContourCL element associated with them, whereas joints have a spline ContourCL element associated with them. The vertebral column has three spline ContourCL elements associated with it, one each for the cervical, thoracic and lumbar regions. A body region or joint can also be associated with a point rather than a line.

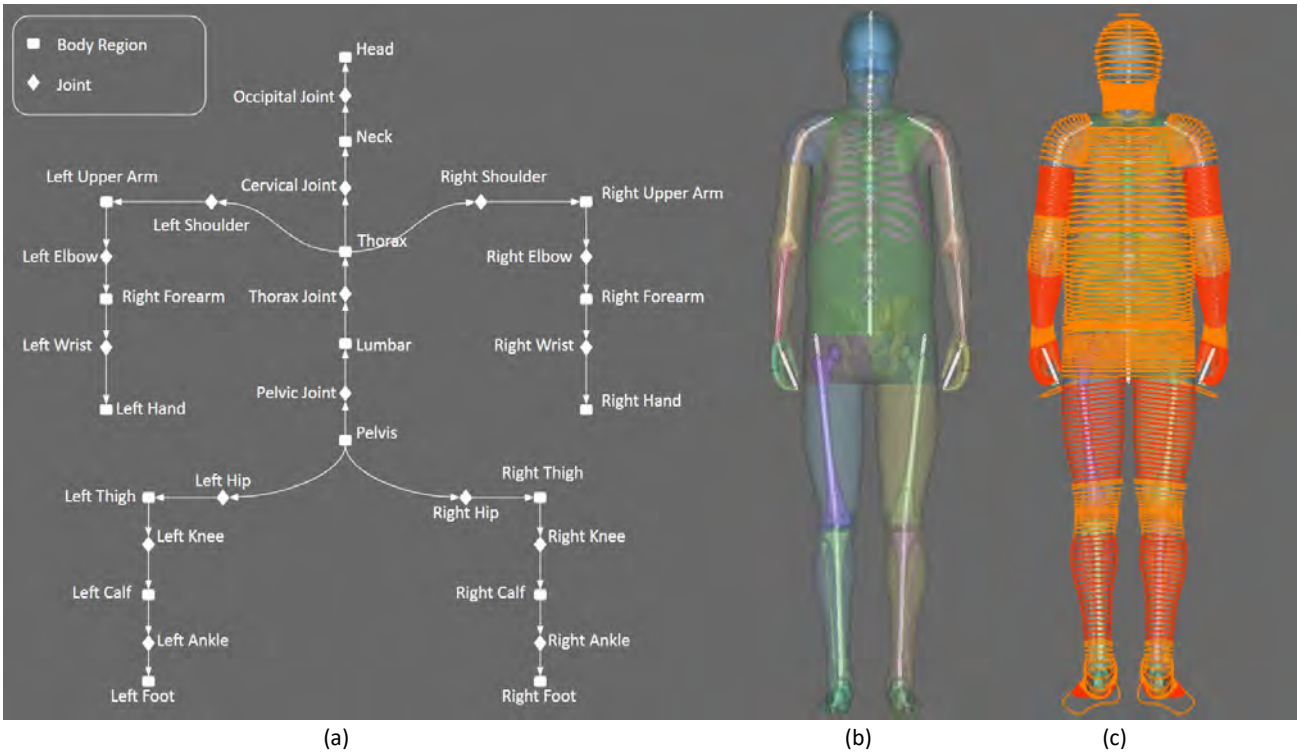

(a) (b) (c)

Fig. 2. (a) The ContourCL tree structure along with (b) the ContourCL curve (white lines inside the HBM), and (c) Contours generated using the ContourCL curve for the THUMS AM50 v4 Pedestrian HBM.

The ContourCL set is stored as a tree data structure (Fig. 2(a)) in which every node is either a body region or a joint. Every joint node has a child body region node, whereas a body region can have many children joint nodes. The root node is the pelvis, registered with the mid superior point on the sacral plate (centre of sacrum). It has three children joints: pelvic joint, left hip and right hip. To illustrate the notion of the CCL, the CCL node of the pelvic joint has the lumbar body region as its immediate child node, which has the thorax joint node as the child node, which in turn has the thorax body region node as its child. The Thorax body region has three child nodes:

the left and right shoulder joints, and the cervical joint. In this manner, all body regions and joints of the body are connected through this CCL structure (Fig. 2(a)).

First, polygonal curves are generated on the HBM by the intersection of the exterior surface of the body with sectional planes perpendicular to the ContourCL curve, consisting of flesh nodes in each plane. Contours are then obtained by scaling these polygonal curves radially outward by 5% to ensure that all HBM nodes are contained inside the surface of these contours (Fig. 2(c)).

Step 2: Delaunay Tetrahedralisation and Node Mapping

Once the contours enclosing the HBM have been generated, Delaunay Tetrahedralisation is carried out for the space enclosed by these contours using TetGen [43]. This generates a partition of the space into a set of tetrahedrons. The partition is a unique partition of the space [44] characterised by the circumsphere of no tetrahedron not containing any other point.

All the HBM nodes inside the space defined by the contours are hence guaranteed to be in exactly one tetrahedron in the generated partition. The nodes are mapped to the respective tetrahedrons they are in, and the *volume coordinates* [45] of the node inside the tetrahedron are computed for use later in the inverse mapping after the contours are translated and rotated for repositioning, as in [37–38][46], or for personalisation.

Step 3: Contour Transformation

This work deals with personalisation of the HBM based on one of the following inputs.

a. Target-based Personalisation: here, target anthropometric parameters are taken as input for personalisation of the HBM. This can be done in one of the following two ways:
   i. given the weight and height as input, a defined set of parameters can be predicted using regression modeling with databases such as the ADULT Dataset (ANSUR) [47], Child Dataset (SNYDER) [48], or Adult Dataset (CCANTHRO) [62];
   ii. if a 3D Human Body surface scan is available, Machine Learning (ML) techniques can be applied to the point cloud to detect the required parameters using a landmarks-based approach [49] or using different parametric models [50-52] along with model registration [53-54].

   Once the target anthropometric parameters are known, factors by which these parameters are to be modified with respect to the original HBM can be computed.

b. Scale-based Personalisation: alternatively, factors to scale length or circumference type anthropometric parameters of individual body segments can be directly used as input to personalise the HBM.

<u>*Length Personalisation*</u>

Body regions of the HBM are separated at specific landmarks on the body skeleton. Contour transformation for length-based personalisation of a body region involves scaling the distance between the contours of the body regions. This involves the following steps.

a) Modification of contours of the body region:

Here, the ContourCL element of the body segment is scaled to the anthropometric measure and the spacing between the contours is changed accordingly.

In this step, the linear and spline-based CCL elements are handled differently. For linear CCL elements, the element length is changed as per the scale factor and the contours are redistributed in the element proportionally. Figure 3((a), (b), (c)) shows how the femur, represented by a linear element in the CCL, is scaled by a factor of 1.2 along its length by uniformly increasing the spacing between them, and translating knee and lower leg contours in the same direction

For the spline element, the shape of the spline needs to be retained to preserve the shape of the body region. Each spine zone is represented as a cubic spline and four control points are associated with it. In order to maintain continuity with adjacent body regions, the slopes at the start and at the end are not altered, and the intermediate control points are repositioned to achieve the desired length. The original contours are then positioned on the modified spline in the same proportion.

Figure 3(d) shows how the knee, represented by a spline element, is scaled by a similar factor. At the start and at the end, the spline representing the knee continues to be tangential to the thigh and the lower leg CCL elements, because the knee CCL element merges with the distal end of the thigh and the proximal end of the lower leg.

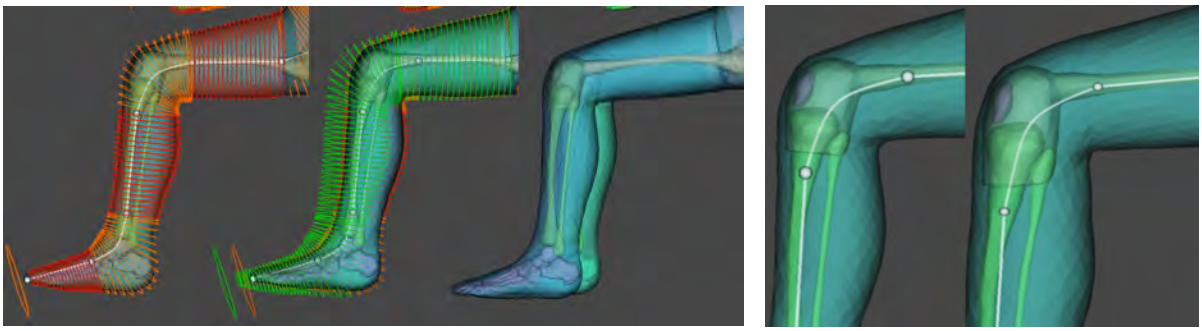

(a) (b) (c) (d)

Fig. 3. For the PIPER Child HBM: (a) Original Left Thigh, its CCL with contours (red), (b) Personalised contours (green): Scaled Left Thigh contours along with translated left knee and lower left leg contours, (c) Scaled Left Thigh with the Right Thigh remaining unscaled, and (d) Knee Spline Length scaled 1.5 times.

b) Translation of child body regions:

Contours of its child segments on the tree are translated as needed. For both the types of CCL elements (linear and spline type), the movement of the last contour is captured, and all child regions are translated by that vector. Figure 3 shows how this is implemented for linear and spline elements, respectively.

Circumference Personalisation

The method of scaling circumference differs from length scaling. Consider the case where the circumferential scaling factor a body region is s_0, and those of the regions adjacent to it are s_1 and s_2 (Fig. 4(a)). In order to maintain continuity at the region interfaces, it is necessary to implement non-uniform scaling of the circumference of the contours. In this work, quadratic interpolation of the circumferential scale factors is done within the above constraints. Figure 4((c), (d)) shows the results when the contours of one of the regions are scaled circumferentially by 1.2 while those of the adjacent regions are not.

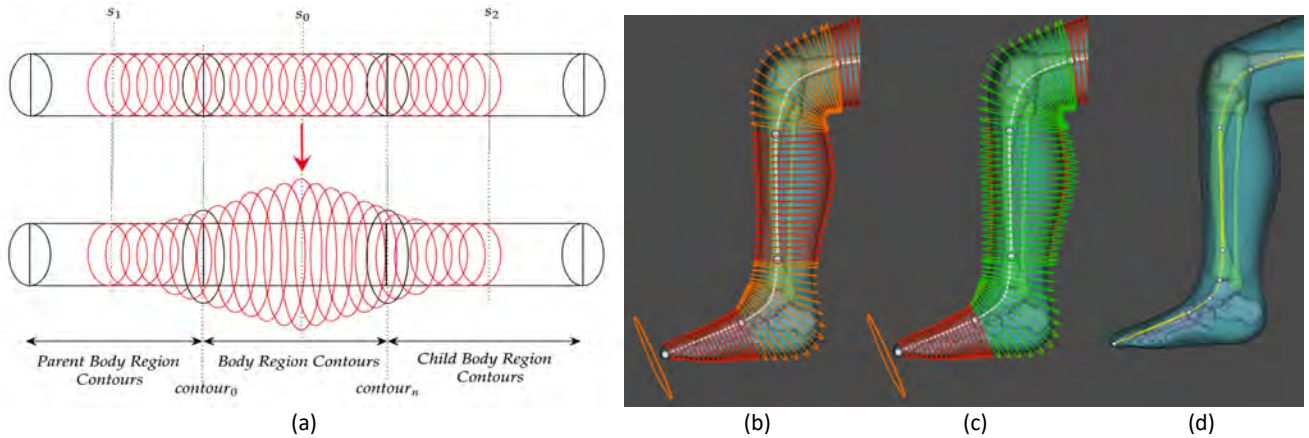

(a) (b) (c) (d)

Fig. 4. (a) Scaling factors of neighbouring body regions, and illustration of non-uniform scaling of contours (for the cases $s_1 < s_0 > s_2$, $s_1 = s_2$); Circumference-based personalisation of the lower leg of the Piper Child HBM: (b) Original Left lower leg, and the CCL with contours, (c) Original (red) and Personalised (green) contours along with original knee and lower leg model, and (d) Left lower leg after scaling.

Step 4: Inverse Delaunay Mapping for Target Model Generation

In this step the flesh and bone nodes are transformed. This step is based on the principles of volume ratio preservation proposed by [37-38][46]. In step 2, a set of Delaunay tetrahedrons and the volume coordinates of all the flesh and bone nodes in these tetrahedrons are computed. At this stage, the contours have been transformed, and the vertices of the tetrahedrons have thus moved. New coordinates of the bone/flesh nodes are then computed using the stored volume coordinates and the modified tetrahedral vertices. Thus, the HBM nodes are repositioned, generating the target-specific HBM.

Step 5: Repositioning Using Target Joint Angles

Once the HBM has been personalised using the anthropometric targets, it is then repositioned to target joint angles using the same contour-based approach used by [39] to generate a posture-specific HBM (PS-HBM). The target joint angles can be obtained from the images or 3-D point clouds of the target human using computer vision and machine learning techniques [55]. Alternatively, these angles can also be obtained from direct physical measurements.

For repositioning at the joints, bones undergo a rigid body transformation. Hence, the Delaunay Tetrahedralisation must be done differently from the case of anthropometric personalisation. Repositioning the HBM at the joint angles requires: (a) calculation of rotation angle using the current joint angle and the target joint angle; (b) Delaunay Tetrahedralisation and mapping of flesh nodes; (c) Contour Deformation as per the joint rotation angles; (d) bone rotations; and (e) Inverse Delaunay Transformation to generate flesh nodes.

a) Calculation of joint rotation angles:
   As previously discussed in Contour Generation, a joint element in the ContourCL tree is a cubic spline. The spline is defined using two end-points (p_1, p_2) and tangent vectors at these points (V_1, V_2). The body region is rotated about the joint's centre and axis of rotation (defined for each joint based on anatomical landmarks). The steps involved are as follows:

   1. Get the points t_1 and t_2 at some distance from p_1 and p_2 along the tangents V_1 and V_2, respectively.
   2. Project t_1 and t_2 on a plane perpendicular to the axis of rotation and get the points T_1 and T_2, respectively (Fig. 5(a)).
   3. Obtain O, the intersection of the axis of rotation and the plane.
   4. Calculate the angle T_1OT_2 and calculate the Joint Rotation Angle as (*Target Joint Angle* $-T_1OT_2$).

b) The Delaunay Tetrahedralisation for repositioning is done similar to that for personalisation. However, since the bones are not to be modified, tetrahedralisation is done using the external contour nodes and the external surface of the bones. As a result, the enclosed space which is the flesh, is partitioned into tetrahedrons. Flesh nodes are then mapped to these tetrahedrons, and the volume coordinates computed as in Step 2.

c) Contour Deformation as per the joint rotation angles:

   The rotation for each contour in the joint region varies with its distance from one end, that is, the spline parameter value (s-value) of that contour. Once the contours are deformed, the flesh nodes between skin and bones are repositioned. The deformation of contours of a joint region depends on the type of joint, the plane of rotation, and the anatomical deformation of skin. Hence, the methods coded for contour deformation change from joint to joint. The process is explained below, using the knee joint flexion as an example.

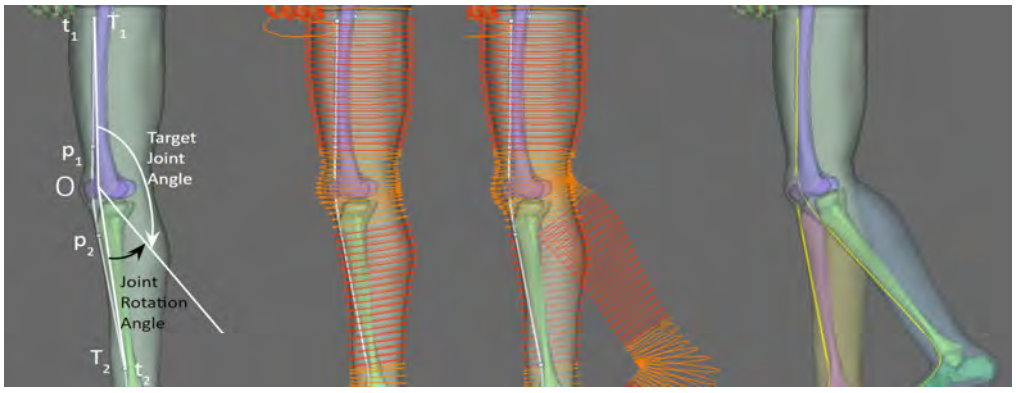

(a) (b) (c) (d)

Fig. 5. Repositioning at the knee joint of THUMS AM50 v4.0 Pedestrian HBM: (a) Joint Rotation Angle Calculation; (b) Contour Generation; (c) Contour Deformation; and (d) Repositioned Knee Joint.

The knee joint spline ContourCL (Fig. 5(a)) is created between the points - P_1, distal femur landmark (DFL) and P_2, proximal tibia landmark (PTL). The knee joint rotation centre is defined by the line joining the medial and lateral condyle landmarks on the femur bone and is used to rotate the lower leg bones. There are 15 contours defined in the knee region. Each of these contours is rotated about the knee joint rotation centre by an amount given by Eq. (1):

$$\theta_i = s_i \cdot \theta \quad (1)$$

where,
$\theta \equiv$ the joint rotation angle
$s_i \equiv$ spline parameter value of the i^{th} contour
$\theta_i \equiv$ rotation angle for the i^{th} contour

The transformed contours are shown in Fig. 5(c).

d) The bones of the lower leg, tibia and fibula are then rotated about the centre of rotation of the knee. The patellofemoral motion includes superior/inferior glide, medial and lateral glide, medial and lateral tilt, and medial and lateral rotation [56]. These motions were measured against tibiofemoral flexion and reported in Zavatsky *et al.* [57]. These data are used to define an affine transformation, which is applied to the patella.
e) At this stage the contours, as well as the bones, have been transformed, the flesh nodes have been mapped in the tetrahedrons created in step 'b' and their volume coordinates are known. New coordinates of the flesh nodes are obtained by inverse mapping using the volume coordinates and the modified locations of the tetrahedral vertices. This completes the rotation at the joint. The leg after rotation at the knee joint is shown in Fig. 5(d).

The Implementation Framework

The Piper Framework [58-59] provides a toolkit for personalisation and repositioning of FE-HBMs. It provides an interface for loading HBMs, interacting with them, and manipulating them. Following are some features available in PIPER:

1. Creating and Exporting Generic Metadata, Landmark Metadata and Entities.
2. Editing and Exporting ContourCL.
3. Regression Module for Anthro Params Prediction.
4. Contour Module consisting of functionalities for –
    a. Contour Generation
    b. Contour based Repositioning
    c. Contour based Personalisation using Uniform Scaling Factor and Using Predicted Anthropometric Parameters
5. Inverse Delaunay Mapping

The current paper describes the contour-based personalisation technique in the PIPER framework, which has been reformulated based on the CCL structure and now works stably to work for all HBMs. It also works directly with 2D/3D images as input, leading to a more robust and efficient methodology with reduced dependence on heuristics.

III. RESULTS

The THUMS AM50 v4 Pedestrian, the GHBMC M50–O, and the THUMS AM50 v7 Occupant HBMs were used to demonstrate the personalisation process. Personalisation was done with a uniform scaling of 10% and 20%, and based on target anthropometric parameters generated by the PIPER Regression Module [60]. The first two demonstrate the personalization process for uniform scaling up to 99 percentile population (20% scaling) and the third case is of non-uniform scaling with specified anthropometry. It is also aimed at demonstrating that the process, which works incrementally for each body region, gives good results and does not produce penetrations or significant distortions at the joints. Table I summarises the cases for which the technique has been demonstrated.

TABLE I
CASES PERSONALISED

Case No.	Base Model	Personalisation target details
1	THUMS AM50 v4 Pedestrian	Target weight 80 kg, Ht 180 cm, Reference database: ANSUR
2	THUMS AM50 v4 Pedestrian	Uniform 10%
3	THUMS AM50 v4 Pedestrian	Uniform 20%
4	GHBMC M50–O	Target weight 80 kg, Ht 180 cm, Reference database: ANSUR
5	GHBMC M50–O	Uniform 10%
6	GHBMC M50–O	Uniform 20%

7	THUMS AM50 v7 Occupant	Target weight 80 kg, Ht 180 cm, Reference database: ANSUR
8	THUMS AM50 v7 Occupant	Uniform 10%
9	THUMS AM50 v7 Occupant	Uniform 20%

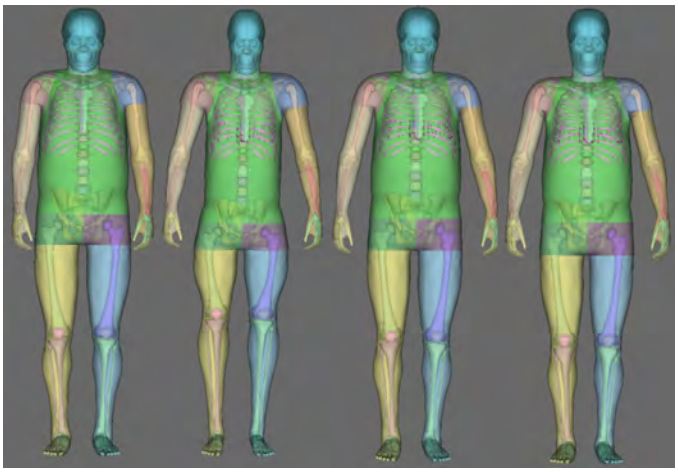

Fig. 7. Left to right: original THUMS v4 AM50 Pedestrian Model (TPM), Target-Personalised TPM (Case 1), TPM Uniformly Scaled by 10% (Case 2), TPM Uniformly Scaled by 20% (Case 3).

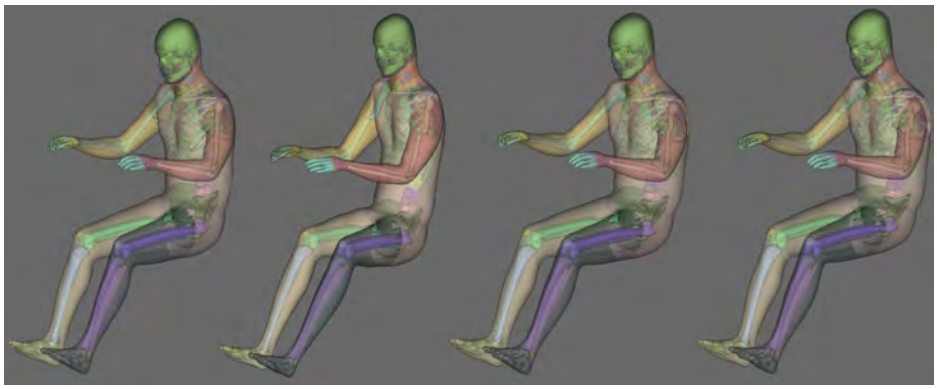

Fig. 8. Left to right: original GHBMC M50–O Model (GM), Target-Personalised GM (Case 4), GM Uniformly Scaled by 10% (Case 5), GM Uniformly Scaled by 20% (Case 6).

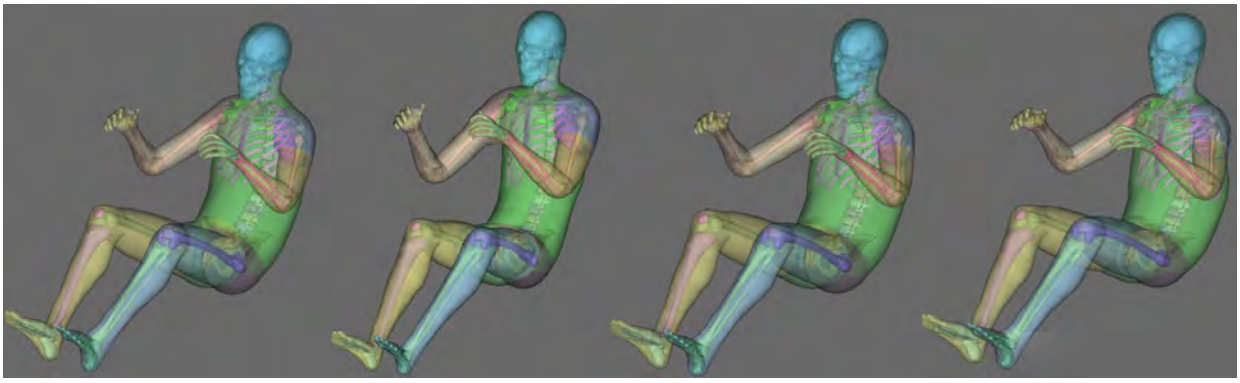

Fig. 9. Left to right: original THUMS v7 AM50 Occupant Model (TOM), Target-Personalised TOM (Case 7), TOM Uniformly Scaled by 10% (Case 8), TOM Uniformly Scaled by 20% (Case 9).

Mesh quality metrics recommended by Burkhart *et al.* [63] for the models generated in the different cases is presented in Tables II–IV. Bad interior angles in the tables II-IV represent angles with large deviation from an ideal angle (60 degrees for tetrahedral elements and 90 degrees for hexahedral elements). In this paper, bad interior angles for tetrahedral elements have been taken to be lying outside the range of 15 to 150 degrees [64-65]. For the hexahedral elements, bad interior angles lie outside the range of 20 to 160 degrees [63].

TABLE II
JACOBIAN MESH QUALITY TABLE FOR PERSONALISED THUMS V4 AM50 PEDESTRIAN HBM
TOTAL NO. OF SHELL ELEMENTS: 443,126

TOTAL NO. OF SOLID ELEMENTS: 1,521,902

Personalisation Case	Minimum Shell Jacobian	% of elements with Jacobian < 0.7	Minimum Aspect Ratio	% of elements with Aspect Ratio < 3	% of tetrahedral elements with bad Interior Angles	% of hexahedral elements with bad Interior Angles
Original Model	0.098	2.38	1.002	2.27	0.0960	0.2890
Case 1: Target Based	0.0975	2.99	1.006	3.22	0.2784	0.3319
Case 2: Uniform Scaling of 10%	0.0927	2.62	1.013	2.47	0.1252	0.3149
Case 3: Uniform Scaling of 20%	0.0925	3.02	1.015	2.69	0.1602	0.3460

7
8

TABLE III
JACOBIAN MESH QUALITY TABLE FOR PERSONALISED GHBMC M50–O HBM
TOTAL NO. OF ELEMENTS CONSIDERED: 643,758
TOTAL NO. OF SOLID ELEMENTS: 1,648,571

Personalisation Case	Minimum Shell Jacobian	% of elements with Jacobian < 0.7	Minimum Aspect Ratio	% of elements with Aspect Ratio < 3	% of tetrahedral elements with bad Interior Angles	% of hexahedral elements with bad Interior Angles
Original Model	0.151	4.54	1.002	7.11	0.5607	1.7649
Case 4: Target Based	-0.351	6.56	1.016	10.66	1.8876	2.2703
Case 5: Uniform Scaling of 10%	0.159	5.13	1.010	7.93	0.6188	1.9161
Case 6: Uniform Scaling of 20%	-0.383	7.32	1.015	9.00	1.1376	2.4924

9
10

TABLE IV
JACOBIAN MESH QUALITY TABLE FOR PERSONALISED THUMS V7 AM50 OCCUPANT HBM
TOTAL NO. OF ELEMENTS CONSIDERED: 452,728
TOTAL NO. OF SOLID ELEMENTS: 1,691,965

Personalisation Case	Minimum Shell Jacobian	% of elements with Jacobian < 0.7	Minimum Aspect Ratio	% of elements with Aspect Ratio < 3	% of tetrahedral elements with bad Interior Angles	% of hexahedral elements with bad Interior Angles
Original Model	0.0988	3.51	1.016	3.18	0.2764	0.3254
Case 7: Target Based	0.0888	5.26	1.031	4.69	0.7791	0.4786
Case 8: Uniform Scaling of 10%	0.0974	3.93	1.029	3.43	0.2931	0.3435
Case 9: Uniform Scaling of 20%	0.0953	4.61	1.022	3.89	0.3561	0.4043

11

The original weights for the THUMS v4 AM50 Pedestrian, GHBMC M50–O, and THUMS v7 AM50 Occupant models are 77 kg, 78.6 kg and 77 kg, respectively, with a stature of 175 cm. The targets used for generating the personalised HBMs (Figs 7–9) are generated from the PIPER regression module using the predictors of weight (80 kg) and stature (180 cm). It is observed that the mesh quality of the whole-body personalised models have small degradation with respect to the original models.

In the case of target-based personalisation, there was an increase of approximately 1.46% in the number of elements with a Jacobian ratio less than 0.7 compared to the baseline model. Additionally, there was an increase of around 2% in the number of elements with an aspect ratio less than 3. For tetrahedral and hexahedral elements, the increase in those with bad interior angles was 0.67% and 0.24%, respectively.

In the 10% uniformly scaled models, only about 0.42% more elements failed the Jacobian and aspect ratio thresholds compared to the baseline. The increase in tetrahedral and hexahedral elements with bad interior angles was 0.035% and 0.065%, respectively.

For the 20% uniformly scaled models, the increase in elements failing the Jacobian and aspect ratio thresholds was 1.51% and 1%, respectively. The additional elements with bad interior angles were around 0.24% for tetrahedral elements and 0.28% for hexahedral elements.

In two of the cases (for the GHBMC M50-O model) the minimum Jacobian in the generated model is negative. We note that for this case the original model had a large number of elements (4.54%) having Jacobian below the usually desired threshold of 0.7 and the number of elements having aspect ratio greater than 3

comprise of nearly 7.11% of total elements in the GHBMC baseline model. This fails the aspect ratio criterion as recommended by [65]. However, the personalisation process maintains the aspect ratio for nearly 90% of the elements in the personalised models. This is certainly a limitation, and ways to improve the results in this case are being investigated.

All the other generated models were tested in the LS-DYNA environment for a stability run for 3ms, and no errors were reported during the same. To further test the suitability of the models, the case I generated model was configured in a car pedestrian crash situation with the Toyota Yaris model [61]. The impact was simulated at 40kmph for a 200ms duration, on the left leg of the pedestrian. The simulation ran successfully, and Fig 10 (a) shows the pedestrian kinematics of the crash during the first 150ms. Failures were observed in the knee ligaments, and in the tibia and fibula bones (Figure 10 (b)). This demonstrates that the generated models are usable in crash simulations.

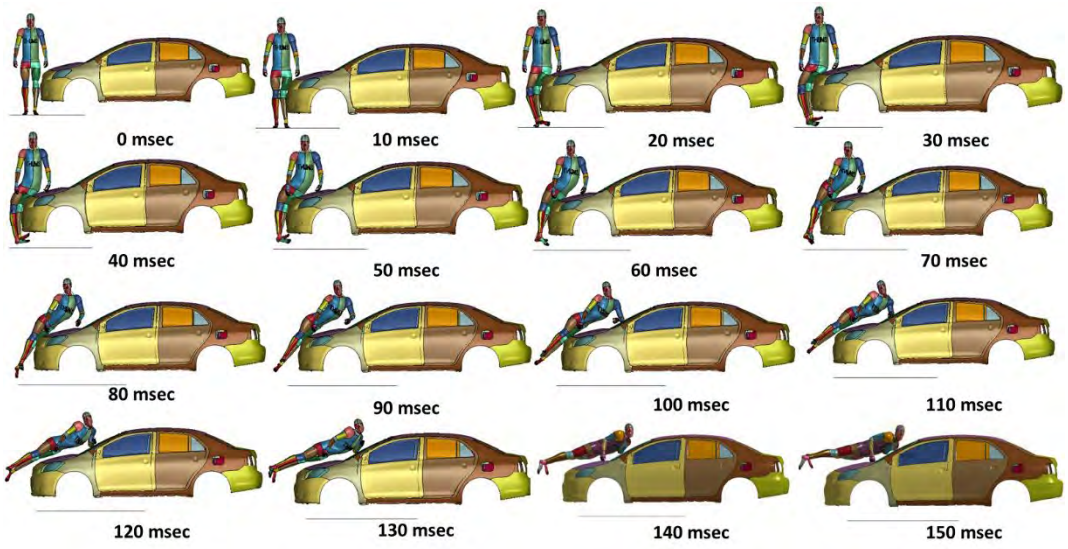

(a)

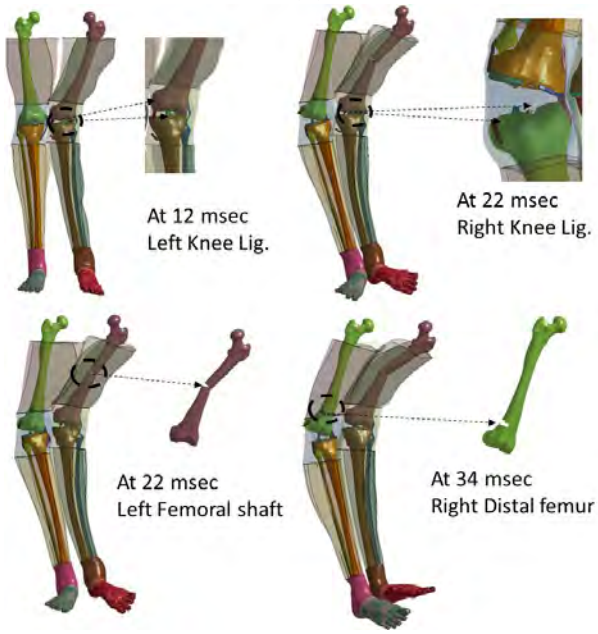

(b)

Fig 10. (a) Kinematics obtained from the car pedestrian crash simulation (b) ligament and bone failures seen during the simulation

IV. DISCUSSION

This approach is implemented and tested for the length and circumference personalisation of the Thigh, Calf, Foot, Lumbar, Thorax, Head, Upper arm, Forearm, Hand Body Regions and Hip, Knee, Ankle, Neck, Shoulder, Elbow, Wrist Joint Regions.

In the initial implementation, each step of personalisation was executed sequentially for all body regions and joints, as per the structure outlined in the ContourCL line. This approach had significant computational demands, and the personalised HBM obtained had a highly distorted mesh with poor mesh quality parameters. This was addressed by implementing a heuristic order that maintained consistent mesh quality during the Delaunay transformation. The ContourCL tree was prepared with this heuristic. Also, the Delaunay Transformation and the inverse mapping were performed only once for the whole HBM instead of repeating these processes for each body region/joint. This optimised process has not only drastically (by as much as 50% in some cases) reduced the computational time, but it was also observed that the elements failing the thresholds of mesh quality metrics were lesser in number. Further, through extensive testing, it was discovered that scaling the length of contours before scaling their circumference during contour personalisation yields better mesh quality.

Hwang *et al.* [28], Jolivet [24] and Janak *et al.* [26] use RBF and Kriging-based techniques to personalise HBMs. They reported [26] that the quality of results improves with the number of control points (landmarks) used. They reported good results when more than 200,000 control points were used. In the method adopted in this paper, only 48 landmarks are used to define the CCL. Consequently, the method is also computationally faster, and it takes only *c.* 60 s to personalise the whole model on an Intel Core i7 CPU with 16 GB of RAM; in the studies [27-28], a time of *c.* 1.5–3 hours was reported for a similar personalisation on an Intel Xeon CPU with 16 GB of RAM. Further, post-processing by mesh optimisation to improve the output mesh quality [26-28][34] is not an essential requirement in the method proposed in this paper because the degradation in the Jacobian is limited to 1% of the elements. It's also worth noting that manual post-processing, as demonstrated by [33], to remove penetrations between elements is time-consuming, typically requiring approximately 4–6 hours per target model. The presented method in this paper does not require manual post-processing for removing penetrations or mesh smoothening.

V. CONCLUSION

This paper describes a contour-based approach for the personalisation of HBMs based on target anthropometric parameters. The methodology generates HBMs with only a minimal difference in the mesh quality of their elements when compared to the original baseline HBM. One significant advantage of the proposed methodology is its ability to perform target-based personalisation on different body and joint regions, as well as scale-based personalisation using a user-defined scaling factor. The generated models can be easily repositioned using target joint angles to represent a given target posture. Also, most of the computations are performed on contour points rather than on the FE mesh, which makes this method computationally fast and makes it feasible to use in practice as a real-time interface.

This contour-based personalisation approach is different from the contour-based repositioning approach [37-39] only in the way Delaunay Tetrahedralisation (DT) and node mapping is performed. While repositioning, the bones undergo only a rigid body motion, while in personalization, their size changes. Hence, for repositioning, the annular region between the skin and the bones needs to go through a non-affine transformation. Hence, during repositioning, the contour nodes as well as the outer surface of the bone serve as reference for DT – to map all flesh nodes in the tetrahedrons generated. During personalization, only the contour nodes are used in the DT stage, so even though bones and flesh are very different in their material properties, they are personalized in the same way.

Since, the bones are not modified explicitly, this method currently does not incorporate the personalisation of bones forms and FE material properties. The bones and internal organs are morphed according to the deformation of contours. Until now, the focus of the work has been the accuracy of target anthropometric parameters, the elemental mesh quality, and to reduce the computational cost of the process. The work of personalisation of bones using the contour-based paradigm is ongoing.

The methodology proposed in this study is implemented in the Contour Module present in the PIPER Software, and the personalised model was used in LS-DYNA to test for stable dynamic simulations.

VI. REFERENCES

[1] Miura, S., Takahashi, S., Parque, V., Miyashita, T. (2021) Small-Scale Human Impact Anthropomorphic Test Device Using the Similarity Rule. *IEEE Transactions on Industrial Electronics*, **68**(8): pp. 7188–7198.

[2] Spethmann, P., Thomke, S., Herstatt, C. (2006) The impact of crash simulation on productivity and problem-solving in automotive R&D. *Working Paper*, No. 43, TUHH, Institute for Technology and Innovation Management, Hamburg.

[3] Mukherjee, S., Chawla, A., Balaraman, K., Soni, A. (2007) Finite element crash simulations of the human body: Passive and active muscle modelling. *Sadhana*, **32**(4): pp. 409–426.

[4] Happee, R., Hoofman, M., Kroonenberg, A. J. V., Morsink, P., Wismans, J. (1998) A mathematical human body model for frontal and rearward seated automotive impact loading. SAE Technical Paper 983150.

[5] Iwamoto, M., Kisanuki, Y., *et al*. (2002) Development of a finite element model of the total human model for safety (THUMS) and application to injury reconstruction. *Proceedings of the IRCOBI Conference*, 2002, Munich, Germany.

[6] Pheasant, S., Haslegrave, C. (2006) *Bodyspace: Anthropometry, Ergonomics and the Design of Work*, p. 352. *CRC Press,* Boca Raton, Florida, USA.

[7] Tejasagar, A., Srikanth, K. V. N. S., Pendyala, V. (2012) Simulation of Vehicular Frontal Crash-Test. *International Journal of Applied Research in Mechanical Engineering*, **2**(1): pp. 262–267.

[8] Bohn, B., Garcke, J., *et al*. (2013) Analysis of Car Crash Simulation Data with Nonlinear Machine Learning Methods. *Procedia Computer Science*, **18**: pp. 621–630.

[9] Hickey, A., Xiao., S. (2017) Finite Element Modeling and Simulation of Car Crash. *International Journal of Modern Studies in Mechanical Engineering*, **3**(1).

[10] Muhammad, A., Shanono, I. H. (2019) Simulation of a Car crash using ANSYS. *15th International Conference on Electronics, Computer and Computation* (ICECCO), 2019, Abuja, Nigeria.

[11] Zalewski, J., Kisilowski, J. (2012) Analysis of Chosen Aspects of a Two-Car Crash Simulation. *Telematics in the Transport Environment*, pp. 34–44.

[12] Maeno, T., Hasegawa, J. (2001) Development of a finite element model of total human model for safety (THUMS) and application to car-pedestrian impacts. *17th International Technical Conference on Enhanced Safety of Vehicles*, 2001, paper 2001-06-0054, Amsterdam, Netherlands.

[13] Shigeta, K., Kitagawa, Y., Yasuki, T. (2009) Development of next-generation human FE model capable of organ injury prediction. *21st International Technical Conference on the Enhanced Safety of Vehicles*, 2009, Stuttgart, Germany.

[14] Iwamoto, M., Kisanuki, Y., *et al*. (2002) Development of a finite element model of the total human model for safety (THUMS) and application to injury reconstruction. *Proceedings of the IRCOBI Conference*, 2002, Munich, Germany.

[15] Iwamoto, M., Nakahira, Y., Kimpara, H. (2015) Development and Validation of the Total HUman Model for Safety (THUMS) Toward Further Understanding of Occupant Injury Mechanisms in Precrash and During Crash. *Traffic Injury Prevention*, **16**(Suppl 1): pp. S36–S48.

[16] Gayzik, F., Moreno, D., Vavalle, N., Rhyne, A., Stitzel, J. (2012) Development of a Full Human Body Finite Element Model for Blunt Injury Prediction Utilising a Multi-Modality Medical Imaging Protocol. *12th International LS-DYNA Conference — Dynalook*, 2012, Detroit, USA.

[17] Serre, T., Brunet, C., *et al.* (2006) HUMOS (Human Model for Safety) Geometry: From One Specimen to the 5th and 95th Percentile. *Proceedings of the SAE Digital Human Modeling for Design and Engineering Conference*, 2006, Lyon, France.

[18] Lindgren, N., Yuan, Q., Pipkorn, B., Kleiven, S., Li, X. (2023) Development and Whole-Body Validation of Personalizable Female and Male Pedestrian SAFER Human Body Models, https://arxiv.org/abs/2305.13918, accessed Dec. 2023.

[19] Pipkorn, B., Jakobsson, L., Iraeus, J., Östh, J. (2023) The SAFER HBM – A Human Body Model for Seamless Integrated Occupant Analysis For All Road Users. *The 27th International Technical Conference on the*

Enhanced Safety of Vehicles (ESV), 2023, Yokohama, Japan.

[20] Beillas, P., Giordano, C., Alvarez, V., Li, X., Ying, X. (2016) Development and performance of the PIPER scalable child human body models. *International Conference on the Protection of Children in Cars, 14th International Conference*, 2016, Munich, Germany.

[21] Chevalier, M.-C., Beillas, P. (2020) Effect of anthropometry scaling on the response of the PIPER child scalable human body model subject to pelvic impact. *Journal of Biomechanics*, **105**: 109757.

[22] Giordano, C., Li, X., Kleiven, S. (2017) Performances of the PIPER scalable child human body model in accident reconstruction. PLoS ONE, **12**(11): e0187916.

[23] Jingwen, H., Fanta, A., Neal, M. O., Reed, M. P., Wang, J.R. (2016) Crash Simulations with Morphed GHBMC Human Models Vehicle Crash Simulations with Morphed GHBMC Human Models of Different Stature, BMI, and Age.

[24] Jolivet, E., Lafon, Y., Petit, P., Beillas, P. (2015) Comparison of Kriging and Moving Least Square Methods to Change the Geometry of Human Body Models. *Stapp Car Crash Journal*, **59**(Nov): pp. 337–357.

[25] Levin, D. (1998) The approximation power of moving least-squares. *Mathematics of Computation*, **67**: pp. 1517–1531.

[26] Janák, T., Lafon, Y., Petit, P., Beillas, P. (2021) A Method to Use Kriging With Large Sets of Control Points to Morph Finite Element Models of the Human Body. *The Journal of Biomechanical Engineering*, **143**(2): 021013.

[27] Hwang, E., Hu J., Reed, M. P., Rupp, J. D. (2015) Development and Application of New Methods for Rapid Development of Diverse Human Models for Crash Simulation, Interim Progress Report, University Of Michigan Transportation Research Institute.

[28] Hwang, E., Hallman, J., *et al.* (2016) Rapid Development of Diverse Human Body Models for Crash Simulations through Mesh Morphing. SAE Technical Paper 2016-01-1491.

[29] Zhang, K., *et al.* (2017) An automated method to morph finite element whole-body human models with a wide range of stature and body shape for both men and women. *Journal of Biomechanics*, **60**: pp. 253–260.

[30] Larsson, K.-J., *et al.* (2019) Evaluation of the Benefits of Parametric Human Body Model Morphing for Prediction of Injury to Elderly Occupants in Side Impact. *Proceedings of the IRCOBI Conference,* 2019, Florence, Italy.

[31] Larsson, K.-J., Pipkorn, B., Iraeus, J., Forman, J., Hu, J. (2021) Evaluation of a diverse population of morphed human body models for prediction of vehicle occupant crash kinematics. *Computer Methods in Biomechanics and Biomedical Engineering*, **25**(10): pp. 1125–1155.

[32] Liu, S., Beillas, P., Ding, L., Wang, X. (2020) Morphing an Existing Open Source Human Body Model into a Personalised Model for Seating Discomfort Investigation. *SAE Technical Paper*, 2020-01-0874.

[33] John, J., Klug, C., Kranjec, M., Svenning, E., Iraeus, J. (2022). 'Hello, world!' VIVA+: A human body model lineup to evaluate sex-differences in crash protection. *Frontiers in Bioengineering and Biotechnology*, **10**: 918904.

[34] Li, X., Yuan, Q., *et al.* (2023) Personalisation of human body models and beyond via image registration. *Frontiers in Bioengineering and Biotechnology*, **11**: 1169365.

[35] Loper, M., Mahmood, N., Romero, J., Pons-Moll, G., Black, M. J. (2015) SMPL: a skinned multi-person linear model. *ACM Transactions on Graphics*, **34**(6): p. 16.

[36] Keller, M., Zuffi, S., Black, M. J., Pujades, S. (2022) OSSO: Obtaining skeletal shape from outside. *Proceedings of the IEEE/CVF conference on computer vision and pattern recognition*, 2022, New Orleans, USA.

[37] Jani, D., Chawla, A., Mukherjee, S., Goyal, R., Vusirikala, N. (2009) Human Body Fe Model Repositioning: A Step Towards Posture Specific - Human Body Models (PS-HBM). *Proceedings of the IRCOBI Conference*, 2009, York, United Kingdom.

[38] Jani, D., Chawla, A., *et al*. (2010) Repositioning the Human Body FE Model at the Knee Joint. *Proceedings of the IRCOBI Conference*, 2010, Hanover, Germany.

[39] Chawla, A., Singh, S., Paruchuri, S., Chhabra, A. (2017) Contour Based Repositioning of Specific Joints of the GHBMC Human Body FE Model. *Symposium on International Automotive Technology*, 2017, Technical Paper 2017-26-0265, Pune, India.

[40] Knupp, P. M. (2000) Achieving finite element mesh quality via optimisation of the Jacobian matrix norm and associated quantities. Part I—A framework for surface mesh optimisation. *International Journal for*

Numerical Methods in Engineering, **48**: pp. 401–420.

[41] Knupp, P. M. (2009) Label-Invariant Mesh Quality Metrics. *Proceedings of the 18th International Meshing Roundtable (IMR)*, 2009, Salt Lake City, UT, USA.

[42] Knupp, P. M. (2000) Achieving finite element mesh quality via optimisation of the Jacobian matrix norm and associated quantities. Part II - A framework for volume mesh optimisation and the condition number of the Jacobian matrix. *International Journal of Numerical Methods in Engineering*, **48**: pp. 1165–1185.

[43] Hang, S. (2015) TetGen, a Delaunay-Based Quality Tetrahedral Mesh Generator. *ACM Transactions on Mathematical Software*, **41**(2): Article 11, p. 36.

[44] Delaunay, B. (1934) Sur la sphère vide. A la mémoire de Georges Voronoi. *Bulletin de l'Académie des Sciences de l'URSS. Classe des sciences mathématiques et na*, (6): pp. 793–800.

[45] Springer, C. E. (1946) Volume Coordinates. *The American Mathematical Monthly*, **53**(7): p. 377.

[46] Jani, D., Chawla, A., Mukherjee, S., Goyal, R., Vusirikala, N. (2009a) Repositioning the Human Body Lower Extremity FE Model. *SAE International Journal of Passenger Cars - Electronic and Electrical Systems*, **2**(1): pp. 1024–1030.

[47] Paquette, S., Gordon, C. C., Bradtmiller, B. (2009) Anthropometric Survey (ANSUR) II Pilot Study: Methods and Summary Statistics.

[48] Snyder, R. G., Schneider, L. W., *et al*. (1997) Anthropometry of Infants, Children, and Youths to Age 18 for Product Safety Design. Highway Safety Research Institute, University of Michigan, USA.

[49] Wang, X., Liu, B., Dong, Y., Pang, S., Tao, X. (2020) Anthropometric Landmarks Extraction and Dimensions Measurement Based on ResNet. *Symmetry*, **12**(12): 1997.

[50] Zuffi, S., Black, M. (2015) The stitched puppet: a graphical model of 3D human shape and pose. *Computer Vision and Pattern Recognition Conference (CVPR),* 2015, Massachusetts, USA.

[51] Baek, S. Y., Lee, K. (2012) Parametric human body shape modeling frame-work for human-centered product design. *Computer Aided Design*, **44**(1): pp. 56–67.

[52] Park, B. K. D., Ebert, S., Reed, M. (2017) A parametric model of child body shape in seated postures. *Traffic Injury Prevention*, **18**(5): pp. 533–536.

[53] Anguelov, D., Srinivasan, P., *et al*. (2005) SCAPE: shape completion and animation of people. *Special Interest Group on Computer Graphics and Interactive Technical Conference, (SIGGRAPH)*, 2005, California, USA.

[54] Hirshberg, D. A., Loper, M., Rachlin, E., Black, M. J. (2012) Coregistration simultaneous alignment and modeling of articulated 3D shape, *12th European Conference on Computer Vision (ECCV),* 2012, Firenze, Italy.

[55] Kusunose, M., *et al.* (2023) Measurement of Shoulder Abduction Angle with Posture Estimation Artificial Intelligence Model. *Sensors* (Basel), **23**(14): p. 6445.

[56] Loudon, J. K. (2016) Biomechanics And Pathomechanics Of The Patellofemoral Joint. *The International Journal of Sports Physical Therapy*, **11**(6): pp. 820–830.

[57] Price, A. J., Oppold, P. T., Murray, D. W., Zavatsky, A. B. (2006) Simultaneous in vitro measurement of patellofemoral kinematics and forces following Oxford medial unicompartmental knee replacement. *The Journal of Bone and Joint Surgery*, **88**(12): pp. 1591–1595.

[58] Beillas, P., Lafon, Y., *et al.* (2017) D3.8 Final version of the personalisation and positioning software tool with documentation. *PIPER EU Project Research Report,* p. 337, IFSTTAR - Institut Français des Sciences et Technologies des Transports, de l'Aménagement et des Réseaux.

[59] Petit, P., Kirscht, *et al.* (2016) Development of an Open Source Framework to position and personalise Human Body Models. *Forty-Fourth International Workshop on Injury Biomechanics Research (NHTSA),* November 2016, Washington DC, USA.

[60] Parkinson, M. B., Reed, M. P. (2010) Creating virtual user populations by analysis of anthropometric data. *International Journal of Industrial Ergonomics*, **40**(Issue 1): pp. 106–111.

[61] Marzougui, D., Samaha, R. R., Nix, L., & Kan, C. D. (2013) Extended Validation of the Finite Element Model for the 2010 Toyota Yaris Passenger Sedan. *Working Paper, NCAC 2012-W-005, National Crash Analysis Center, The George Washington University.*

[62] Robinette, K., Blackwell, S., Daanen, H., Boehmer, M., Fleming, S. (2002) Civilian American and European Surface Anthropometry Resource (CAESAR). *Final Report*, Volume **1**, p. 74.

[63] Burkhart, T. A., Andrews, D. M., Dunning, C. E. (2013) Finite element modeling mesh quality, energy balance and validation methods: A review with recommendations associated with the modeling of bone

tissue. *Journal of Biomechanics*, *46*(9), pp. 1477–1488

[64] Shewchuk, J.R., Labelle, F. (2007) Tetrahedral mesh generation with good dihedral angles using point lattices. *University of California, Berkeley*.

[65] Foteinos, P. A., Chrisochoides, N. P. (2013). High-Quality multi-tissue mesh generation for finite element analysis. Soft Tissue Biomechanical Modeling for Computer Assisted Surgery, Springer, pp. 157-176.